Polymer 295 (2024) 126742

Contents lists available at ScienceDirect

Polymer

journal homepage: www.elsevier.com/locate/polymer

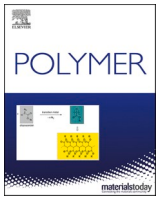

Combining oscillatory shear rheometry and dynamic mechanical analysis to obtain wide-frequency master curves

Ábris Dávid Virág [a], Zsolt Juhász [a], Attila Kossa [b], Kolos Molnár [a,c,d,*]

[a] Department of Polymer Engineering, Faculty of Mechanical Engineering, Budapest University of Technology and Economics, Műegyetem rkp. 3., H-1111, Budapest, Hungary
[b] Department of Applied Mechanics, Faculty of Mechanical Engineering, Budapest University of Technology and Economics, Műegyetem rkp. 3., H-1111, Budapest, Hungary
[c] HUN-REN-BME Research Group for Composite Science and Technology, Műegyetem rkp. 3., H-1111, Budapest, Hungary
[d] MTA-BME Lendület Sustainable Polymers Research Group, Műegyetem rkp. 3., H-1111, Budapest, Hungary

ARTICLE INFO

Keywords:
Time–temperature superposition
DMA
Rheology
Shear sandwich clamp
Shear modulus
Mastercurve

ABSTRACT

In this paper, we present a novel approach combining widely available techniques, oscillatory shear rheometry and dynamic mechanical analysis to obtain wide-frequency range master curves. We carried out finite element analysis to investigate the influence of the specimen thickness and Poisson's ratio on the moduli measured with a shear sandwich clamp in solid-state. We demonstrated that the thickness/height ratio of the specimen greatly influences its shear stress state. Using polystyrene, which is a thermorheologically simple thermoplastic, we showed that continuous master curves can be generated from melt-state torsion and solid-state shear tests. Our results can facilitate the characterisation of polymers from viscous to elastic state and the development of test methods that use more accurate calculations.

1. Introduction

Polymers are viscoelastic materials, i.e. they exhibit both liquid-like (viscous) and solid-like (elastic) properties. Consequently, their rheological properties are time- and frequency-dependent [1].

There are many applications where wide-frequency rheological data are used to deduce molecular structure. This rheological behaviour is significantly influenced by the molecular weight and dispersity, as well as by their molecular architecture, e.g. chain branching [2]. Therefore, by using reptation theory-based models, it is possible to estimate the frequency-dependent rheological behaviour of entangled linear polymers from their molecular weight distribution (direct problem) [3] or to predict the molecular weight distribution from their wide-frequency rheological data (inverse problem) [4]. Although the latter is an ill-posed problem, it can be solved by an efficient numerical algorithm or by postulating the unknown molecular weight distribution with suitable functions, e.g. by generalized exponential (GEX) distribution functions [5–7]. Schanbag [8] used a Bayesian data analysis technique to solve the inverse problem and developed an algorithm, which can be useful for identifying unknown linear and star polymers and blends based on their frequency-dependent rheological behaviour. In the case of polymers with complex architecture, wide-frequency rheological data can be an excellent complement to classic characterisation techniques such as size exclusion chromatography, and it can be used to validate an assumed structure [9].

Wide-frequency rheological data can also be used to support the engineering design. Pelayo et al. [10] fitted a Prony-series to the wide-frequency master curves of polyvinyl butyral (PVB) and used the results to simulate the mechanical response of a laminated glass element containing PVB layers to dynamic loading. Fenton et al. [11] designed and synthesised 12 conjugated polymers with aromatic backbones, then used the characteristic points of wide frequency master curves (e.g. plateau modulus and Rouse time of an entanglement strand) to propose a simple crossover equation between Kuhn-length, Kuhn monomer volume and the plateau modulus. Their findings can greatly facilitate the design of implantable bioelectronics. Cai et al. [12] used wide-frequency rheological data to validate a so-called brachiation model which they proposed. The model can link the molecular-scale properties with bulk mechanics for dynamically associating polymer networks, which can be used as self-healing materials.

* Corresponding author. Department of Polymer Engineering, Faculty of Mechanical Engineering, Budapest University of Technology and Economics, Műegyetem rkp. 3., H-1111, Budapest, Hungary.
E-mail address: molnar@pt.bme.hu (K. Molnár).

https://doi.org/10.1016/j.polymer.2024.126742
Received 5 December 2023; Received in revised form 22 January 2024; Accepted 25 January 2024
Available online 6 February 2024

Determining frequency-dependent rheological properties over a wide frequency range requires a multi-step test and analysis process. The two widely used instruments for the characterisation of viscoelastic materials are oscillatory shear rheometers for polymer melts and solutions [13,14] and dynamic mechanical analysers (DMA) for solids [15–18]. These instruments typically have a measurement range 0.01–100 Hz, but characterising a polymer's rheological behaviour from ideally viscous to ideally elastic requires a range of 10–15 decades. Some oscillatory shear rheometers can accurately measure at frequencies lower than 0.01 Hz [19–21]. However, these tests could take days or even weeks, and this long time can lead to changes in material structure, e.g. the degradation of the sample, which can affect the results.

To extend the measurement range, instead of long-term tests, a widely used method is to apply the time–temperature superposition (TTS) principle [22,23], described in detail by Ferry [24]. Materials to which TTS can be used are called thermorheologically simple [25]. TTS is based on analogue effects, e.g. both increasing the test temperature and decreasing the test frequency soften polymers the same way. The changes in material properties (e.g. modulus) between solid-like and liquid-like behaviour are of several orders of magnitude. Therefore, describing rheological behaviour from the viscous to the glassy state with a single instrument can be difficult. One possible solution to this problem is small-diameter parallel-plate (SDPP) rheometry [26]. Mangal et al. [27] used this method to characterise the viscoelastic behaviour of polymer–nanoparticle composites over a wide frequency range of 10–14 decades, from viscous to elastic behaviour, with a 3 mm diameter parallel plate fixture. Zhong et al. [28] used pairs of plates with 8 and 4 mm diameters to systematically study the linear viscoelastic behaviour of polystyrene (PS) melts and solutions over a 10-decade frequency range, from viscous to elastic behaviour. However, due to the finite torsional stiffness of the parts of the rheometer, a correction of instrument compliance is required, and in this case, even a small deviation in test specimen size can cause a significant error [29].

The other option to extend the frequency range of dynamic rheological tests is to convert the results of creep tests performed in the time domain into the frequency domain [30,31]. The advantage of the method is that it can be used even when TTS is not applicable. However, the obtained results depend on the conversion method used. In addition, during the creep test, the sample is exposed to high temperatures for a long time, which can lead to degradation, affecting the results. Furthermore, finding the stress required for linear viscoelastic (LVE) creep tests can be time-consuming, as several preliminary creep tests are needed to map the independence of creep compliance from the applied stress. He et al. [32] carried out the complete LVE characterisation of two, branched polypropylenes having long relaxation times by combining oscillatory shear data with creep data. You and Yu [33] used this method to determine the LVE behaviour of PMMA-based nanocomposites over a wide frequency range.

Another option for extending the measurement range is to use special instruments such as subresonant piezo rheometers, bulk resonators or ultrasound rheometers to investigate the rheological behaviour of polymers up to 10^8 Hz [34]. Athanasiou et al. [35] presented a piezoelectric sliding-plate rheometer, which is suitable for testing viscoelastic and fragile samples from 10 Hz to 1 kHz. Szántó et al. [36] used a conventional rheometer combined with a piezoelectric rotary vibrator and a quartz resonator to determine the rheological behaviour of various polyethylene, poly(vinyl acetate) and poly(ethylene-co-vinyl acetate) copolymer samples in a broad frequency range, including the MHz range. These techniques are typically used to complement the conventional testing methods and can also be used even when TTS is not applicable. However, these are usually custom-built instruments and are not widely available.

The aim of this study is to develop a feasible method for obtaining the rheological properties of thermoplastic polymers over the widest frequency range possible. For this purpose, we chose widely available instruments (oscillatory shear rheometer and DMA). We chose polystyrene, a thermorheologically simple, amorphous, linear homopolymer widely studied in rheology literature as the model material. Using simplified mechanical models of the different loading modes, we showed that a continuous master curve can be constructed from melt-state torsion and solid-state shear tests. The proposed method is suitable for exploring the relationships between flow properties and molecular structure, and it can also be used to optimise processing.

2. Materials and methods

2.1. Concept

The frequency-dependent rheological behaviour of an amorphous, linear thermoplastic polymer can be divided into four regions: the terminal, the rubbery plateau, the transition and the glassy regions. The boundaries of these regions are defined by the crossover points of the storage and loss modulus curves (Fig. 1/a). At low frequencies, the loss modulus (G'') dominates over the storage modulus (G'), therefore the material exhibits viscous behaviour (δ is close to 90°), while at very high frequencies, the material behaves elastically, with G' dominating (δ being close to 0°). The viscoelastic nature of an amorphous, linear thermoplastic polymer can be clearly understood if the phase angle (δ) is plotted as a function of the absolute value of the complex modulus ($|G^*|$). This way, we obtain the so-called van Gurp-Palmen (vGP) plot [37], also known as the Booij-Palmen plot [38] (Fig. 1/b).

To characterise a polymer from ideally elastic to ideally viscous behaviour, an extensive temperature range is required: a set of experiments should be carried out starting from temperatures below the glass transition temperature (T_g) to temperatures above the flow temperature. However, this requires a carefully thought out solution, which can provide reliable results despite the significant change in modulus due to temperature changes.

Therefore, we investigated whether the rheological shear properties (see Supplementary Section S1) measured in the solid state with a DMA and in the melt state with an oscillatory shear rheometer can be pooled to obtain the frequency-dependent rheological behaviour from the ideally viscous to the ideally elastic state. We examined the applicability of this novel method based on theoretical mechanical considerations and experimental tests.

The main idea is that the vGP plot is closely related to molecular structure, independent of temperature and of frequency (except at the glass transition region). Practice shows that the measurement of the total vGP curve of an amorphous thermoplastic polymer usually cannot be carried out with a single measurement setup. Assuming ideal measuring instruments and conditions, frequency sweep test results obtained at different temperatures and/or frequencies will provide different sections of the same polymer-specific vGP curve. Therefore, different instruments can be used to obtain the different sections of this curve. To obtain the total vGP curve accurately, there has to be an overlap between the resulting curves measured with different instruments in the terminal or the rubbery plateau region. Based on the total vGP curve obtained from frequency sweeps, the rheological behaviour of the examined thermoplastic polymer can be characterised over the widest frequency range possible.

2.2. Material and sample preparation

The polystyrene (PS) used in this study was a general-purpose grade, Edistir N 3840 (supplied by Versalis, San Donato Milanese, Italy) with a Young's modulus of 3250 MPa (at room temperature), a density of 1.05 g/cm^3 and an MFI (200 °C/5 kg) of 10 g/10 min according to the manufacturer's data. The number (M_n) and weight average (M_w) molecular weight of this material are 119.3 and 221.3 kg/mol, respectively (measured for this research by gel permeation chromatography). For the tests, we made 160 mm × 160 mm sheets by compression moulding at

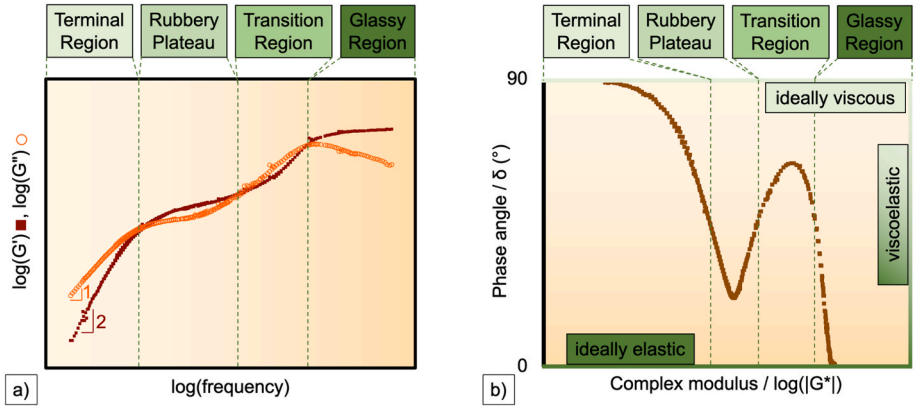

Fig. 1. Theoretical frequency-dependent storage (G′) and loss modulus (G) curves (a) and the van Gurp-Palmen ~~diagram~~ plot (b) for an amorphous, linear, thermoplastic homopolymer.

220 °C with a Teach-Line Platen Press 200E (Dr. Collin GmbH, Munich, Germany) machine using 0.5-1-, 2-, 3- and 4-mm thick steel press frames. The steps of moulding were the following: i) the press plates were preheated at 0 MPa for 3 min, ii) the raw material (PS) was loaded into the press frame and preheated for 1 min without applying pressure, iii) the sheets were pressed at 5 MPa hydraulic pressure (pressure on the sample surface was 0.625 MPa) for 1 min, iv) the sheets were pressed at 10 MPa hydraulic pressure (pressure on the sample surface was 1.25 MPa) for 1 min, v) the sheets were pressed at 20 MPa (pressure on the sample surface was 2.5 MPa) for 3 min, vi) the sheets were cooled down with water cooling of the press plates and removed from the press when the temperature of the mould reached 30 °C. Between the first four steps, the mould was opened and closed back again for outgassing.

We injection moulded type 1A dumbbell-shape specimens (ISO 527–2:2012) on an Arburg Allrounder Advance 270S 400-170 machine (Arburg GmbH, Lossburg, Germany) using a conventional two-cavity cold-runner mould for tensile tests to determine the Poisson's ratio. The barrel zone temperatures from hopper to nozzle were 40, 205, 210, 215, 220 and 220 °C.

The mould was tempered to 30 °C. The shot volume was 45 cm^3, and the injection rate was 44 cm^3/s. After injection, a holding pressure of 500 bar was applied at an injection rate of 20 cm^3/s. The clamping force was 400 kN.

2.3. Measuring the average molecular mass

Gel permeation chromatography/size exclusion chromatography (GPC/SEC) analyses were performed using a method described in Molnar et al. [39].

2.4. Melt state tests (dynamic rheological analysis)

To investigate the rheological properties of the PS samples in melt state, we used an MCR-301 (Anton-Paar, Graz, Austria) oscillatory shear rheometer in a parallel-plate geometry setup with a plate diameter of 25 mm and a gap size of 1 mm. Small amplitude oscillatory shear (SAOS) tests were carried out at 160, 200 and 240 °C. The compression moulded sheets were cut into small pieces with pliers for the tests. After loading the samples, a 3-min retention time was applied to allow relaxation processes to take place and achieve thermal equilibrium. We carried out controlled-strain frequency sweeps with a strain amplitude of 5 %, which was in the linear viscoelastic region (LVER), as verified by strain amplitude sweeps. Frequency sweeps were performed in the 0.01–100 Hz frequency range with 10 points/decade with logarithmic scoring in every case.

2.5. Solid state tests (dynamic mechanical analysis, DMA)

To investigate the dynamic mechanical behaviour at temperatures at which the PS was already acting like a solid and, therefore, could no longer be tested with a conventional oscillatory shear rheometer setup, we carried out dynamic mechanical analysis (DMA) with a DMA Q800 device (TA instruments, New Castle, DE, USA) and a shear sandwich clamp. We cut 10 × 10 mm samples from the 1, 2, 3 and 4 mm thick pressed sheets using a utility knife. Strain and frequency sweep tests (described below) were performed on the sheets.

To validate the results from the shear tests, especially in the temperature range below the glass transition temperature, we carried out dynamic tests in tensile mode. We cut 30 mm × 3 mm rectangular specimens from the 0.5 and 2 mm thick pressed sheets and performed the strain and frequency sweeps using a film tension clamp with a 10 mm gripping distance. Below 100 °C, we used 0.5 mm thick specimens, but above 100 °C, due to a significant decrease in Young's modulus, we used 2 mm thick specimens, and unlike at other frequency sweeps, we reduced the frequency range from 1–100 Hz to 1–40 Hz to achieve accurate results.

In all cases, tests were carried out in oscillation mode. After loading the samples, we set the temperature, and upon reaching it, we applied a 3-min retention time to allow relaxation processes to take place and achieve thermal equilibrium. We carried out controlled-strain frequency sweeps in the frequency range of 1–100 Hz in every case (except for tests in a tensile arrangement above 100 °C) using 10 points/decade with logarithmic scoring. The frequency sweeps were carried out at different temperatures, between 60 and 150 °C in shear mode, and from 30 to 130 °C in tensile mode, in 10 °C steps. In some cases, we reduced the steps to 5 °C to get more detailed results where more significant changes occurred. The strain amplitudes were changed with temperature to ensure linear viscoelastic responses, as verified by strain amplitude sweeps.

2.6. Determining the Poisson's ratio

The Poisson's ratio was determined at different temperatures with uniaxial tensile tests on the injection moulded specimens. A Z250 universal tensile tester (Zwick Gmbh., Ulm, Germany) was used, equipped with a temperature chamber, a 20 kN load cell with a resolution of 0.1 N and 20 kN rated Zwick 8355 screw grips. The gripping distance and crosshead speed was 115 mm and 1 mm/min, respectively. Three tests were carried out at the following temperatures each: 30, 50, 70, 90, 110 and 130 °C. The longitudinal and lateral elongation of the specimens were measured with a Mercury Monet (Sobriety, Kurim, Czech Republic) digital image correlation–based optical strain measuring system using a data acquisition rate of 20 Hz, equipped with a 5 MP camera and

two LED lights. The longitudinal and transverse gauge were 50- and 7-mm-long line probes, respectively, with a facet size of 25 × 25 pixels. The Poisson's ratio was determined from the longitudinal and lateral strain curves plotted as a function of time. First, we cut the initial, uncertain sections of the curves, then we fit a linear function to the remaining, steady slope part of each curve. Finally, we calculated the Poisson's ratio (ν) as the negative ratio of the slopes of the longitudinal ($a_{\varepsilon\parallel}$) and lateral ($a_{\varepsilon\perp}$) strain curves (Eq. (1)):

$$\nu = -\frac{a_{\varepsilon\perp}}{a_{\varepsilon\parallel}}. \tag{1}$$

2.7. Model fittings

The WLF model was fitted according to the method of Oseli et al. [40]. All model fittings were performed with the least squares method in the Matlab R2022a software (Mathworks, Natick, MA, USA).

3. Results and discussion

3.1. Mechanical models of the different loading modes

This section summarises the mechanical relationships of the test configurations under investigation. Fig. 2 presents the simplified mechanical models for three different test setups: uniaxial tensile test (a), shear sandwich test (also known as double lap shear test) (b), and torsion test (c).

In the case of the uniaxial tensile test and shear sandwich test, the test specimen had a rectangular prism geometry, while in the case of the torsion test, the specimen had a cylindrical shape. The geometric dimensions in their undeformed state are depicted in Fig. 2. In uniaxial tensile testing, the clamping force exerted by the grips slightly deformed the test specimen, an effect that was neglected in subsequent calculations. In shear and torsion configurations, ideal contact was assumed between the test specimens and the gripping structure. During uniaxial tensile loading, far from the grips, the strain and stress state of the test specimen can be considered approximately homogeneous. However, in the case of torsion loading, the stress and strain state within the material is non-homogeneous. In the shear configuration, the accuracy of the simplified relationship introduced for stress calculation greatly depends on the thickness of the test specimen. Section 3.2 provides a detailed analysis of this effect.

In an actual DMA experiment, the prescribed displacements are small compared to the dimensions of the test specimens. Therefore, an accepted approximation for describing the mechanical behaviour of the material during these tests is the theory of small strains and deformations. For uniaxial tensile loading, we denote the applied displacement as Δl, for shear, it is Δu, and for torsion, the angular displacement is $\Delta\varphi$. Eqs. (2)–(4) show the characteristic stress and strain for each loading condition. To distinguish these quantities, different subscripts are employed: U for uniaxial, S for shear, and T for torsion.

$$\sigma_U = \frac{F_U}{A_U} = \frac{F_U}{ab}, \varepsilon_U = \frac{\Delta l}{l}, \tag{2}$$

$$\tau_S = \frac{F_S}{A_S} = \frac{F_S}{2cw}, \gamma_S = \frac{\Delta u}{t}, \tag{3}$$

$$\tau_T = \frac{M_T}{I_p}\rho = \frac{4M_T}{r\pi^4}\rho, \gamma_T = \frac{\Delta\varphi}{h}\rho. \tag{4}$$

In Eq. (4) I_p represents the polar second moment of area of the circular cross-section and ρ is the radial coordinate in the torsion test. To describe purely elastic material behaviour, we use Hooke's law (Eq. (5)). The Young's modulus (E) is related to the shear modulus (G) via the expression $E = 2G(1+\nu)$, where ν is the Poisson's ratio. Then, the shear modulus of the material can be calculated from the measured force (Eq. (6)) and torque (Eq. (7)) as:

$$\sigma_U = E\varepsilon_U \rightarrow G = \frac{l}{2ab(1+\nu)}\cdot\frac{F_U}{\Delta l} = k_U\cdot\frac{F_U}{\Delta l}, \tag{5}$$

$$\tau_S = G\gamma_S \rightarrow G = \frac{t}{2cw}\cdot\frac{F_S}{\Delta u} = k_S\cdot\frac{F_S}{\Delta u}, \tag{6}$$

$$\tau_T = G\gamma_T \rightarrow G = \frac{4h}{r\pi^4}\cdot\frac{M_T}{\Delta\varphi} = k_T\cdot\frac{M_T}{\Delta\varphi}, \tag{7}$$

where parameters k_U, k_S and k_T are the "geometry factors" commonly used in testing devices to consider the effect of geometry. The measuring instruments use Eqs. (5)–(7) to calculate modulus. Note that uniaxial tensile test gives the Young's modulus. In the shear configuration, there is no analytical solution to this elasticity problem when considering actual geometries and boundary conditions. The simplified formula (Eq. (6)) is only an approximation, which holds true as $t \rightarrow 0$. Therefore, we examine the shear sandwich test in detail from a mechanical point of view in Section 3.2.

3.2. Investigating the mechanical aspects of the shear sandwich test

During a shear mode DMA test, both the strain and stress fields are non-homogeneous within the material [41]. Furthermore, the solution to the elasticity boundary value problem implies that stress concentration occurs in the corners, causing stress to approach infinity in these regions [42].

Clearly, real materials cannot endure such stress concentrations.

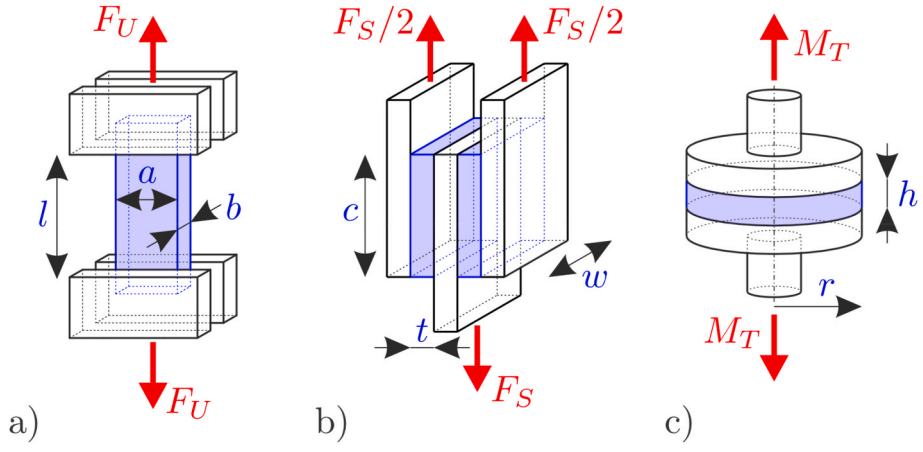

Fig. 2. Schematics of the investigated loading modes: a) uniaxial tensile b) shear sandwich c) torsion.

There are two extreme scenarios regarding the thickness of the test specimen: when the thickness is significantly smaller than the other dimensions (thin test specimen) and when it is substantially larger. Fig. 3 shows the von Mises stress distribution in a thinner ($t/c = 0.3$) and a thicker ($t/c = 3.0$) specimen. The colours represent different magnitudes of stress. The results were obtained with finite element simulations with a fine mesh utilizing eight-node plane strain elements. The primary purpose of Fig. 3 is to illustrate the non-homogeneous stress field within the specimens. For this, arbitrary material parameters can be used, therefore the details of the finite element model are not discussed here.

For thinner test specimens, the approximate formula for shear (Eq. (6)) can be employed, since t is close to zero. In contrast, for thicker test specimens, the geometry of the test specimen more closely resembles that of a beam, and in this case, the relationship between displacement and force is expressed with the use of well-known principles from the strength of materials [43]. By rearranging this relationship, we can express G (Eq. (8)):

$$\Delta u = \frac{1}{2}\cdot\frac{F_S t^3}{12IE} = \frac{1}{2}\cdot\frac{F_S t^3}{wc^3 2G(1+\nu)} \rightarrow G = \frac{1}{2}\cdot\frac{t^3}{2(1+\nu)wc^3}\cdot\frac{F_S}{\Delta u}. \tag{8}$$

where I represents the second moment of area about the bending axis. It is evident that the resulting relationship is fundamentally different from the formula obtained for a thin test specimen. To illustrate the effect of geometry, let us introduce the dimensionless parameter $\eta = t/c$, which expresses the ratio of thickness (length) to the height of the test specimen. In this case, by substituting η into (Eq. (6)) and (Eq. (8)), the relationships for the shear modulus become:

$$G_{thin} = \frac{1}{2}\cdot\frac{\eta}{w}\cdot\frac{F_S}{\Delta u}, G_{thick} = \frac{1}{2}\cdot\frac{\eta^3}{2(1+\nu)w}\cdot\frac{F_S}{\Delta u}. \tag{9}$$

To distinguish between the two different G values, we have denoted them with distinct subscripts in the equations. The ratio of the G values calculated with the two different methods is described by a quadratic function in terms of η (Eq. (10)):

$$\frac{G_{thick}}{G_{thin}} = \frac{\eta^2}{2(1+\nu)}. \tag{10}$$

The two expressions for G yield the same value when $\eta = \sqrt{2(1+\nu)}$. For instance, when $\nu = 0.3$, η equals 1.61, while for $= 0.5$, η equals 1.73. For a real test specimen geometry, the value of η is neither zero nor infinite—the formulas in Eq. (9) provide an inaccurate estimation of G. There is no analytical closed-form solution to the elasticity boundary value problem for the $F_S(\Delta u)$ relationship. We can provide an asymptotic solution only within the singularity region. However, for us, it is crucial to establish the relationship between the displacement applied to the structure and the resulting force. To precisely determine the effect of the thickness of the test specimen on the calculated value of G with the assumption of homogeneous deformation, we constructed a finite element model and determined the relationship between the applied force and displacement for various thicknesses and Poisson's ratios. With this information, we can gain a detailed understanding of the error associated with G obtained under the assumption of homogeneous deformation. The detailed description of the finite element model can be found in Appendix B.

During the finite element analysis, we assigned the shear modulus in the model and obtained the F_S values corresponding to the prescribed Δu displacement. With the use of these virtual data, the shear modulus can be calculated with the formulas corresponding to the two extreme scenarios. The relative error of the two formulas is determined by the formulas in Eq. (11):

$$e_{thin} = \frac{G_{thin} - G}{G}\cdot 100\ (\%), e_{thick} = \frac{G_{thick} - G}{G}\cdot 100\ (\%). \tag{11}$$

The change in relative errors with respect to η for various values of ν is illustrated in Fig. 4.

The first significant observation is that in both cases of applying the formulas, a smaller G value is obtained than the actual G value of the material. It can also be observed that the error of the formula corresponding to thin test specimens tends to approach zero as η approaches zero. The error of this formula has an approximately linear dependence on η in the $\eta = 0\ldots1$ range. For specimens typically used for conventional DMA, the maximum inaccuracy due to geometrical dimensions is about 10 %, and the effect of Poisson's ratio is small within this range. Therefore, at a fixed test specimen length, using a thinner specimen will result in a more accurate result, but the maximum measurable modulus

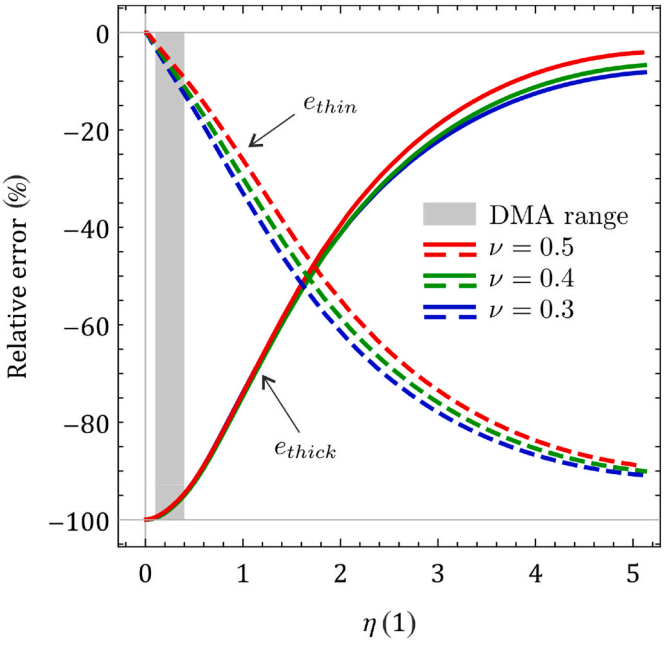

Fig. 4. Relative errors of the simplified formulas for different values of the Poisson's ratio.

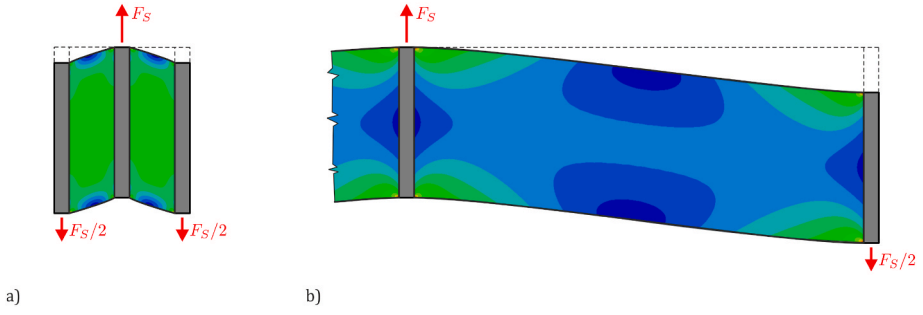

Fig. 3. von Mises equivalent stress distribution for a thinner ($t/c = 0.3$) and a thicker ($t/c = 3.0$) specimen.

will also be smaller (see Eq. (6)). On the other hand, this formula results in significant errors for thick test specimens. For instance, at $\eta = 1$ and $\nu = 0.3$, the relative error is approximately -27%. This effect is in contrast to the other formula, which provides a zero G value for $\eta \to 0$, causing the relative error to converge to -100%. However, the error tends to approach zero as the thickness of the test specimen increases. In this case, the influence of the Poisson's ratio is not negligible. Our results show that it is preferable to use test specimens with an $\eta \leq 0.4$ or $\eta \geq 4.6$ because neither of the two formulas gives accurate results in the intermediate range.

Most DMAs work with the $\eta < 0.4$ range, but the numerical results obtained in this manner can be utilised to more accurately account for the geometry effect in calculations, and can facilitate the development of novel test methods, e.g. van't Hof et al. [44] designed a clamp with $\eta = 5$, which can accurately measure materials with high stiffness.

3.3. Master curve generation method

In this section, we present the method we developed through tests. The idea is to construct a master curve from two different test methods. In solid state, we carried out frequency sweep tests with the DMA in shear mode (S), and in the melt state, we performed tests with an oscillatory shear rheometer in torsion mode (T). The results obtained from these two tests should give us the same modulus (see Supplementary material Section S3).

First, we plotted the van Gurp-Palmen (vGP) plots from each test (Fig. 5/a). The curves produced with the same instruments are consistent, but in relation to each other, they are not. There are two regions in the vGP curve, where significant scattering can be observed: around the local minimum (δ_{min}) and the local maximum (δ_{max}). The scattering around δ_{min} and the lower moduli obtained by DMA is probably because DMA shear tests in the solid state are affected by several errors such as material defects (bubbles, inclusions, inhomogeneity, surface defects), non-ideal shear stress conditions and non-ideal contact between clamp and sample (risk of slippage). In a strain-controlled test, the actual strain of the material may be smaller than the assumed strain due to possible slippage. Therefore, the instrument assumes a larger strain for a given stress, thus the measured modulus is smaller than the actual modulus. The scattering around δ_{max} is due to the α-relaxation process, which is associated with glass transition, and which is a frequency-dependent phenomenon [45], therefore as the frequency increases, the α-relaxation peak shifts to higher temperatures and higher peak values.

The master curves are generated with the use of TTS (see Supplementary material S2), which can be done if the vGP plot is continuous. To create a continuous vGP curve, we shifted the curves to the curve that contains δ_{min}. The abscissa of the δ_{min} point can be considered the plateau modulus (G_N^0), which is a characteristic parameter [46]. However, two different δ_{min} values were obtained from the two different tests (Table 1). The difference between the ordinate values of δ_{min} is less than 1 %, while the difference between the abscissa values is 75 %. Since the shape of the curve matches the shape of a typical vGP curve of an amorphous thermoplastic polymer and the difference between the ordinate values of δ_{min} is minimal, it can be concluded that the phase shift values are adequate, but modulus correction is needed.

Based on the literature, PS materials have a plateau modulus of around $2 \cdot 10^5$ Pa [47]. The $1.5 \cdot 10^5$ Pa, obtained from torsion mode tests, is close to this value, but to verify the accuracy, we carried out further analysis. Based on the empirical relationship found by Trinkle and Friedrich [48] we estimated the weight average molecular weight (M_w) by Eq. (12) using $\rho = 1050\ \mathrm{kg/m^3}$ and $A = 1$ (Table 1):

$$M_w = M_e \cdot 10^{\frac{1.91 - \log \delta_{min}}{0.61}} = A \frac{\rho RT}{G_N^0} \cdot 10^{\frac{1.91 - \log \delta_{min}}{0.61}}, \tag{12}$$

Table 1
Parameters of the two different δ_{min} values and calculated molecular weights.

	Measured data			Calculated values	
	T (K)	G_N^0 (Pa) (abscissa)	δ (°) (ordinate)	M_e (kg/mol)	M_w (kg/mol)
DMA	423.15	82,219	21.86	44.9	386.9
Oscillatory shear rheometer	433.15	143,835	21.57	26.3	231.3

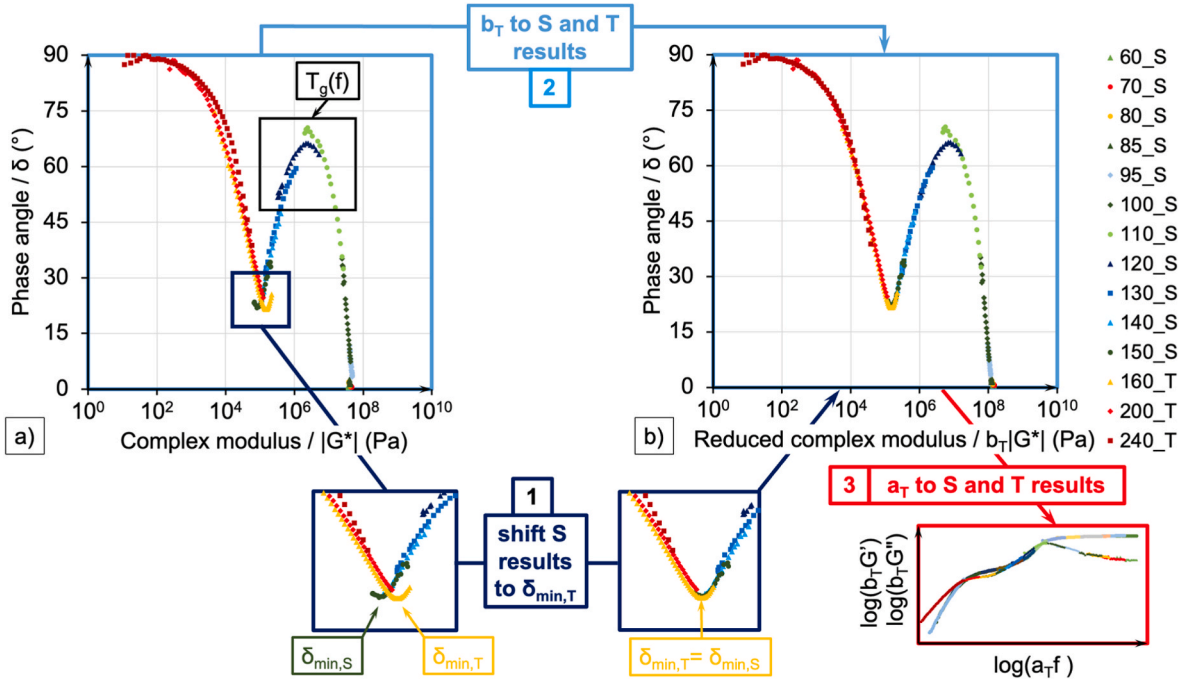

Fig. 5. The master curve generation method: unadjusted (a) and adjusted (b) van Gurp-Palmen ~~diagram~~ plot of the curves measured at different temperatures. The legends indicate the test temperature. S stands for shear tests using DMA and the T stands for torsion mode test using the oscillatory shear rheometer.

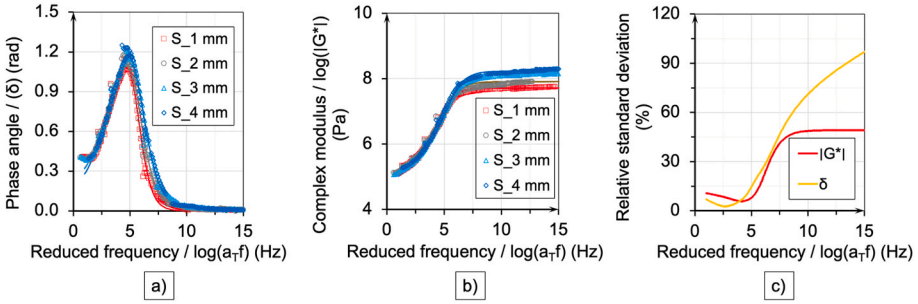

Fig. 6. The shear mode (S) part of the generated master curves at T_{ref} = 160 °C and the fitted models (continuous lines) for the phase angle (a) and the complex modulus (b), and the relative standard deviations (c). Relative standard deviation was calculated as the ratio of the standard deviation to the mean.

where M_e (kg/mol) is the entanglement molecular weight. M_e is a phenomenological parameter, which cannot be measured, only inferred [49]. A is a molecular model–dependent constant (Trinkle and Friedrich used $A = 1$ $A = 1$ in their calculations), ρ (kg/m^3) is the density of the polymer at T (K), which is the absolute temperature at which the G_N^0 was measured, $R = 8.314$ J/(mol·K)$R = 8.314$ J/(mol · K) is the universal gas constant.

The two M_w estimates differ significantly, but the M_w estimated from the torsion mode tests differs only 4.5 % from the $M_w = 221.3$ kg/mol, which was obtained from gel permeation chromatography (GPC).

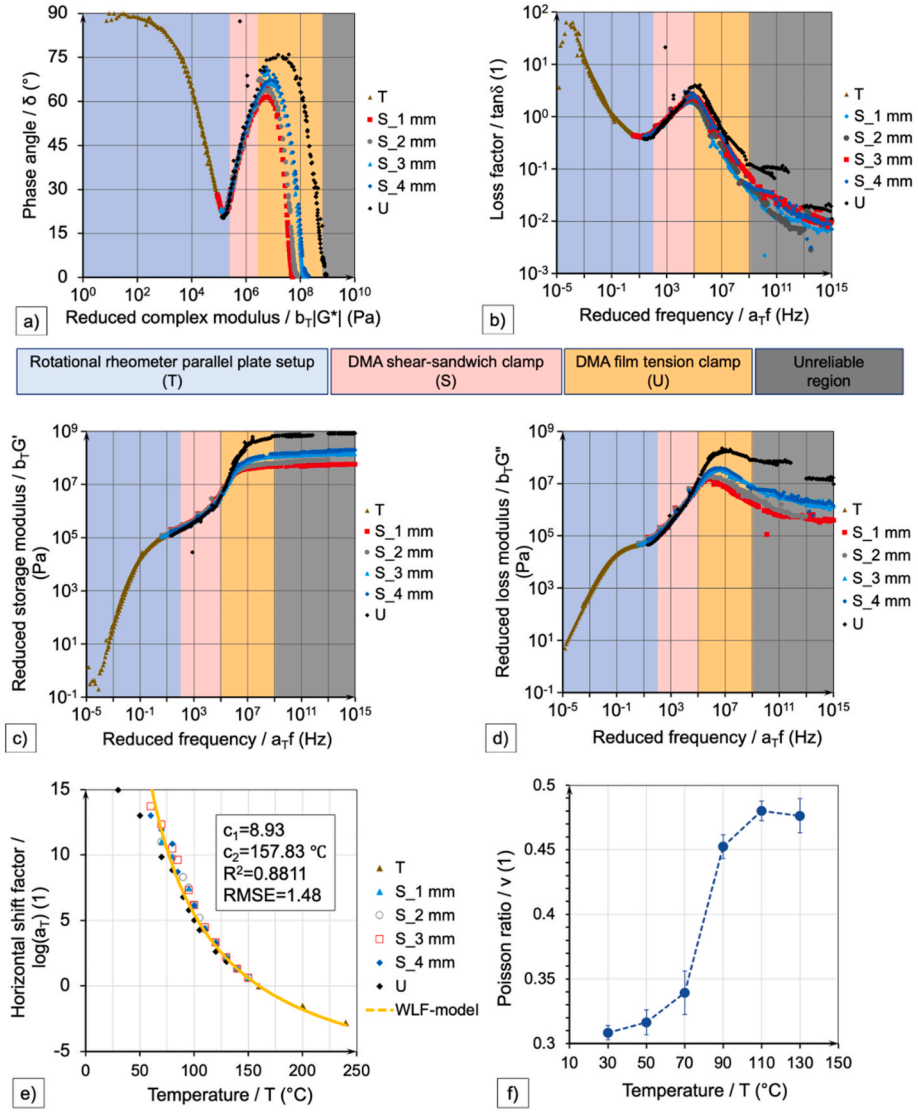

Fig. 7. Results of the performed master curve generation using 160 °C as a reference temperature: a) vGP plot, b) loss factor, c) storage modulus, d) loss modulus, e) temperature dependence of the horizontal shift factor, f) temperature dependence of the Poisson's ratio. The legends indicate loading modes: T stands for torsion mode test using the oscillatory shear rheometer, S stands for DMA shear tests and U stands for DMA uniaxial tensile tests. The ranges of applicability are arbitrary and apply only to the PS material tested.

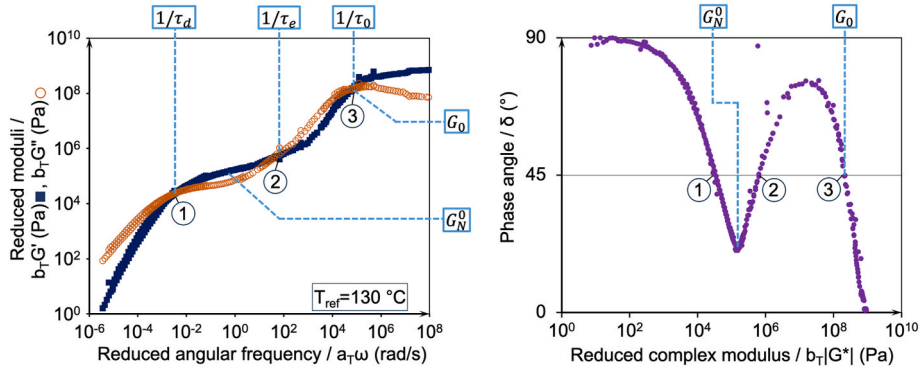

Fig. 8. Rheological plots obtained as a result of the master curve generation method for the tested PS material: frequency-dependent storage (G′) and loss modulus (G) curves at $T_{ref} = 130$ °C (a) and the van Gurp-Palmen plot (b).

Therefore, the curve measured in torsion mode containing δ_{min} should be chosen for accurate results. Using this curve as the reference, we first adjusted the vGP curves measured in shear mode, and then applied a modulus shift factor (b_T) (Fig. 5/b). This resulted in the continuous vGP curve, allowing the master curve to be constructed with appropriate horizontal shift factors (a_T). Using the method described by Dealy and Plazek [50], we carried out manual horizontal shifting until we reached a superposition that resulted in a continuous plot.

3.4. Wide-frequency master curves

To investigate the influence of specimen thickness on the shear test results, we performed this method on 1-, 2-, 3- and 4-mm thick sheets. Based on the finite element analysis results regarding thickness (Section 3.2.), this falls into $\eta = 0.1 - 0.4$, therefore we used the formula for thin specimens (Eq. (6)). The measured results were corrected with the e_{thin} relative error obtained from the finite element analysis (Section 3.2) and the effect of the Poisson's ratio was also taken into account.

To test the consistency of the results obtained from tests of specimens of different thicknesses we fitted sigmoidal models to the shear mode (S) part of the generated $|G^*(f)|$ and $\delta(f)$ master curves based on the study of Liu and Luo [51]. The shear mode (S) part of the master curves and the fitted models are shown in Fig. 6/a-b and the model parameters are given in Supplementary material Section S5. Based on these models, we determined the relative standard deviation along the whole frequency range (Fig. 6/c). We defined 10^5 Hz ($log(a_T f) = 5$ Hz) as an upper limit of the application range of the shear mode tests, because at this point the relative standard deviation for δ and $|G^*|$ is 15 % and 8 %, respectively.

After defining these limits, the master curves were drawn. The results of the master curve construction performed are shown in Fig. 7. In Fig. 7/a-d, the range of applicability of each test method is indicated with different colours. Note that these ranges are based on an arbitrarily chosen level of deviation, but it clearly defines the different ranges.

The adjusted vGP plots of these tests are shown in Fig. 7/a. The curves are approximately identical up to the δ_{max} (around $|G^*| = 10^7$ Pa), but there are significant differences above that modulus. The results obtained from the DMA shear sandwich clamp (S) can expand the result of rheometry (T) by about 3 decades (from 10^2 to 10^5 Hz) based on both the storage modulus (Fig. 7/a), loss modulus (Fig. 7/b) and loss factor (Fig. 7/c) curves.

Over 10^5 Hz (in the vicinity of the local maximum of the loss factor, which can be related to the α-relaxation and glass transition) sample thickness affects the results of the tests. Fig. 7/b shows that the drastic differences occur at about the peak of the loss factor curve. At this point the material is in a brittle, glassy state, making DMA clamping unstable and possibly slipping.

We also examined the temperature dependence of the shift factors. The WLF equation holds for the whole range (Fig. 7/e), besides, the shift factors still fit the WLF model when the shear sandwich clamp is no longer applicable. Thus, although this model is often used to verify the applicability of the superposition itself, it is not suitable for verifying the accuracy of the master curves, because it cannot detect the error in modulus.

Although, the vGP curve is continuous (Fig. 7/a), the WLF dependence of the shift factors holds over the whole measurement range (Fig. 7/e), and the master curves look continuous in every case (Fig. 7/b-d) the moduli show a significant variation in the glassy region for different specimen thicknesses. Therefore, these methods only provide information about the goodness of superposition, i.e. the continuity of the master curve. The inaccurate modulus values are not always filtered by these methods, because these methods verify the curves only qualitatively (the shape of the curve), not quantitatively (the exact values). Therefore, additional considerations are needed to validate the master curve in the glassy region.

For this reason, we carried out tensile mode tests. For a homogeneous, isotropic material, Young's modulus (determined from a tensile test at temperatures below T_g at low test speeds) is equal to the frequency-dependent storage modulus at very high frequencies. The tensile modulus values obtained from these tests were converted to shear modulus by Eq. (5). with the use of the temperature-dependent Poisson's ratios measured with tensile tests (Fig. 7/f). Fig. 7/b-d also shows that the uniaxial tension clamp (U) can be used to extend the results even further, up to 7 decades (up to about 10^9 Hz) compared to oscillatory shear rheometry, but above this value the results from the uniaxial test are quite unreliable.

The Young's modulus of the PS used is 3250 MPa at room temperature, which is roughly equivalent to a shear modulus of 1000 MPa (10^9 Pa) obtained with the use of the Poisson's ratio of 0.31 measured at 30 °C (Fig. 7/e). The storage modulus curve obtained with the tension clamp is approaching this realistic modulus value.

It can be concluded that for homogeneous, isotropic materials, this method can significantly extend the results obtained with oscillatory shear rheometry. Moreover, in the case of isotropic materials, it is advisable to use a tension clamp or a shear sandwich clamp with $\eta \geq 4.6$ to characterise the rheological properties over the widest frequency range possible (up to the glassy state). For anisotropic materials (e.g.

Table 2
The set of rheological parameters determined from the obtained master curve at $T_{ref} = 130$ °C.

	Parameter	Value determined from master curve
τ_d	disentanglement or reptation time	318.5 s
τ_e	Rouse time of entanglement strand	0.025 s
τ_0	Rouse time of Kuhn segment	$1.57 \cdot 10^{-5}$ s
G_0	Kuhn modulus	137.7 MPa
G_N^0	Plateau modulus	0.144 MPa

composites), if master curve construction is applicable, this method also can be used, but additional mechanical considerations are required because the rheological properties of composites are orientation-dependent.

Overall, this method can be used to construct wide frequency range master curves that can describe the frequency-dependent behaviour of thermorheologically simple materials from the ideally viscous state up to the ideally elastic state.

3.5. Material parameter set directly obtainable from the wide-frequency master curves

The wide frequency curves obtained as a result of the master curve generation method for $T_{ref} = 130$ °C are shown in Fig. 8/a. The figure shows that there is no region in the plateau zone (between the first and second crossover points) where the G' is truly horizontal. Moreover, the G' curve has several inflexion points. These indicate that the tested PS is an entangled, polydisperse polymer [47].

The frequency-dependent plot has three clearly identifiable points at the intersections of the G' and the G'' curves. Point coordinates can be used to determine a number of specific moduli and time parameters that can be applied in rheological models, e.g. tube theory-based models. In our case, the plateau modulus can only be clearly identified on the van Gurp-Palmen plot. Based on these points' coordinates, the polymer's complex rheological behaviour can be reduced to a data set of a few parameters (Table 2), which are suitable for investigating polymer melts' chain dynamics. Our results are in good agreement with the findings of Zhong et al. [28] reported on different polystyrene melts and solutions.

These parameters can be used to investigate the chain dynamics of polymers, which are of great importance in the simulation of polymer processes. Szuchacs et al. [52] used the reptation time (obtained from the first crossover point) to predict the bonding strength between the two coupled parts during overmoulding, which is a special injection moulding process. Robertson et al. [53] used the reptation time and Rouse time of chain (calculated using the first and second crossover points) to simulate the extrudate swell of polystyrenes. Kearns et al. [54] used the Kuhn relaxation time (which can be derived from the third crossover point) to develop a new methodology which is suitable to describe the effect of flow on the crystallisation kinetics of polyethylene after processing has occurred. Overall, the method presented in this study is suitable for investigating the frequency-dependent rheological behaviour of thermoplastic polymers over a wide range of frequencies, which allows us to explore the relationships between flow properties and molecular structure and to optimise processing.

4. Conclusion

We present a novel method to characterise the shear rheological properties of thermorheologically simple, thermoplastic polymers in a wide frequency range. The method combines oscillatory shear rheometry and dynamic mechanical analysis (DMA). We investigated the mechanical aspects of a shear sandwich clamp using finite element analysis. We found that specimen thickness and Poisson's ratio, which is highly temperature-dependent, have significant effects on the modulus obtained. These results can be used to better account for the effects of geometry in calculations and can facilitate the development of new test methods.

We carried out shear tests on PS material in the melt and the solid state using oscillatory shear rheometry with a parallel-plate setup and a DMA equipped with a shear sandwich clamp, respectively. Using the results from the two different tests, we adjusted the vGP curve to be continuous, then master curves were created with the use of time-temperature superposition. To validate the results, we also performed tests using a DMA tensile clamp. The moduli obtained in tensile mode were converted to shear moduli with the measured Poisson's ratios. We found that the DMA shear sandwich clamp can be used to extend the master curve obtained with a conventional parallel plate rheometer, by 3 decades. However, extensibility is limited by the measurement range of the clamp setup. The use of a clamp with a thickness/height ratio greater than 4.6 can be a solution to this problem, and the rheological properties of thermorheologically simple, thermoplastic polymers can be characterised over the widest frequency range possible. Rheological curves obtained this way can be used to characterise the molecular structure and can be implemented in simulations.

CRediT authorship contribution statement

Ábris Dávid Virág: Writing – original draft, Visualization, Methodology, Investigation, Formal analysis, Data curation, Conceptualization. **Zsolt Juhász:** Investigation, Formal analysis, Data curation. **Attila Kossa:** Writing – original draft, Visualization, Investigation. **Kolos Molnár:** Writing – review & editing, Supervision, Funding acquisition.

Declaration of competing interest

The authors declare that they have no known competing financial interests or personal relationships that could have appeared to influence the work reported in this paper.

Data availability

Data will be made available on request.

Acknowledgements

The research reported in this paper was supported by the National Research, Development and Innovation Office (FK 138501 and FK 142457). Project no. TKP-6-6/PALY-2021 has been implemented with the support provided by the Ministry of Culture and Innovation of Hungary from the National Research, Development and Innovation Fund, financed under the TKP2021-NVA funding scheme. The authors are grateful for the kind help of Kristóf Molnár and the Biomacromolecular Engineering Research Group at the College of Food, Agricultural, and Environmental Sciences of The Ohio State University in the GPC/SEC analysis.

Appendix A. Supplementary data

Supplementary data to this article can be found online at https://doi.org/10.1016/j.polymer.2024.126742.

Appendix B. Finite element analysis for the shear sandwich test

The primary geometric characteristic of the finite element model is the dimensionless value of $\eta = t/c$. In our case, $w = c$. The ultimate goal of the analysis was to determine the relationships between the computed and specified G values. Actual geometry has no influence on this ratio, only the value of η. Furthermore, the Poisson's ratio also affects the results. Thus, a particular finite element model can be characterized by two dimensionless parameters: ν and η. In our case, $w = c = 10$ mm, and we vary the value of t. Of the material properties, we set $G = 1$ GPa and vary the value of the

Poisson's ratio. We incremented the value of η from 0.01 to 5.12 with intervals of 0.01. We discretised the geometry with 3D brick elements. Following a mesh independence study, we adopted a meshing strategy where 25 quadratic elements (C3D20) were applied along each edge. In the case of $\nu = 0.5$, we employed hybrid elements (C3D20H) due to volumetric incompressibility. In this scenario, 15625 quadratic elements were used for each model, resulting in a total of 68276 nodes. The displacements of the nodes on the lower surface of the test specimen were constrained in all directions, while for the nodes on the upper surface, we prescribed the displacement Δu in the shear direction, with all other displacement components set to zero. The sum of reaction forces was extracted, which provides F_S. From these values, the shear modulus can be calculated. The finite element simulations were performed with Abaqus version 2022.

References

[1] R. Boyd, G. Smith, Polymer Dynamics and Relaxation, Cambridge University Press, Cambridge, 2007, https://doi.org/10.1017/CBO9780511600319.

[2] E. Van Ruymbeke, H. Lee, T. Chang, A. Nikopoulou, N. Hadjichristidis, F. Snijkers, D. Vlassopoulos, Molecular rheology of branched polymers: decoding and exploring the role of architectural dispersity through a synergy of anionic synthesis, interaction chromatography, rheometry and modeling, Soft Matter 10 (2014) 4762–4777, https://doi.org/10.1039/c4sm00105b.

[3] E. van Ruymbeke, R. Keunings, V. Stéphenne, A. Hagenaars, C. Bailly, Evaluation of reptation models for predicting the linear viscoelastic properties of entangled linear polymers, Macromolecules 35 (2002) 2689–2699, https://doi.org/10.1021/ma011271c.

[4] E. Van Ruymbeke, R. Keunings, C. Bailly, Determination of the Molecular Weight Distribution of Entangled Linear Polymers from Linear Viscoelasticity Data, 2002.

[5] M.R. Nobile, F. Cocchini, A generalized relation between MWD and relaxation time spectrum, Rheol. Acta 47 (2008) 509–519, https://doi.org/10.1007/s00397-007-0228-1.

[6] F. Léonardi, A. Allal, G. Marin, Molecular weight distribution from viscoelastic data: the importance of tube renewal and Rouse modes, J Rheol (N Y N Y) 46 (2002) 209–224, https://doi.org/10.1122/1.1428315.

[7] V. Ianniello, S. Costanzo, R. Pasquino, G. Ianniruberto, V.K. Gupta, L. Stieglitz, B. Rieger, T. Tervoort, N. Grizzuti, Evaluating the molecular weight distribution of ultrahigh molecular weight polypropylene through rheology, Phys. Fluids 35 (2023) 063108, https://doi.org/10.1063/5.0147911.

[8] S. Shanbhag, Analytical rheology of blends of linear and star polymers using a Bayesian formulation, Rheol. Acta 49 (2010) 411–422, https://doi.org/10.1007/s00397-010-0443-z.

[9] X. Chen, H. Lee, M.S. Rahman, T. Chang, J. Mays, R. Larson, Analytical rheology of asymmetric H-shaped model polybutadiene melts, Macromolecules 45 (2012) 5744–5756, https://doi.org/10.1021/ma300337x.

[10] F. Pelayo, M.J. Lamela-Rey, M. Muniz-Calvente, M. López-Aenlle, A. Álvarez-Vázquez, A. Fernández-Canteli, Study of the time-temperature-dependent behaviour of PVB: application to laminated glass elements, Thin-Walled Struct. 119 (2017) 324–331, https://doi.org/10.1016/j.tws.2017.06.030.

[11] A.M. Fenton, R. Xie, M.P. Aplan, Y. Lee, M.G. Gill, R. Fair, F. Kempe, M. Sommer, C.R. Snyder, E.D. Gomez, R.H. Colby, Predicting the plateau modulus from molecular parameters of conjugated polymers, ACS Cent. Sci. 8 (2022) 268–274, https://doi.org/10.1021/acscentsci.1c01396.

[12] P.C. Cai, B. Su, L. Zou, M.J. Webber, S.C. Heilshorn, A.J. Spakowitz, Rheological characterization and theoretical modeling establish molecular design rules for tailored dynamically associating polymers, ACS Cent. Sci. 8 (2022) 1318–1327, https://doi.org/10.1021/acscentsci.2c00432.

[13] Gebhard Schramm, 3 - types of rheometers/viscometers, in: A Practical Approach to Rheology and Rheometry, Thermo Electron (Karlsruhe) GmbH, Karlsruhe, 2004, pp. 28–77.

[14] A. Ghanbari, Z. Mousavi, M.C. Heuzey, G.S. Patience, P.J. Carreau, Experimental methods in chemical engineering: rheometry, Can. J. Chem. Eng. 98 (2020) 1456–1470, https://doi.org/10.1002/cjce.23749.

[15] K.P. Menard, N. Menard, 5 - dynamic testing and instrumentation, in: Dynamic Mechanical Analysis, third ed., CRC Press, Boca Raton, 2020, pp. 85–110.

[16] I.R. Henriques, L.A. Borges, M.F. Costa, B.G. Soares, D.A. Castello, Comparisons of complex modulus provided by different DMA, Polym. Test. 72 (2018) 394–406, https://doi.org/10.1016/j.polymertesting.2018.10.034.

[17] K.S. Kumar, S. Gairola, I. Singh, Sustainable polymers and sisal fibers based green composites: a detailed characterization and analysis, Express Polym. Lett. 17 (2023) 992–1006, https://doi.org/10.3144/expresspolymlett.2023.74.

[18] B. Öztürk, T. Inan, H. Atakül, F.S. Guner, Smart polyurethane composites: magnetic-field-sensitive crosslinked shape-memory polyurethane composites, Express Polym. Lett. 17 (2023) 660–673, https://doi.org/10.3144/expresspolymlett.2023.48.

[19] S. Perni, P. Prokopovich, Rheometer enabled study of cartilage frequency-dependent properties, Sci. Rep. 10 (2020) 20696, https://doi.org/10.1038/s41598-020-77758-9.

[20] P.A. Rühs, C. Affolter, E.J. Windhab, P. Fischer, Shear and dilatational linear and nonlinear subphase controlled interfacial rheology of β-lactoglobulin fibrils and their derivatives, J Rheol (N Y N Y) 57 (2013) 1003–1022, https://doi.org/10.1122/1.4802051.

[21] C. Berlangieri, G. Poggi, S. Murgia, M. Monduzzi, L. Dei, E. Carretti, Structural, rheological and dynamics insights of hydroxypropyl guar gel-like systems, Colloids Surf. B Biointerfaces 168 (2018) 178–186, https://doi.org/10.1016/J.COLSURFB.2018.02.025.

[22] V. Dorléans, R. Delille, D. Notta-Cuvier, F. Lauro, E. Michau, Time-temperature superposition in viscoelasticity and viscoplasticity for thermoplastics, Polym. Test. 101 (2021), https://doi.org/10.1016/j.polymertesting.2021.107287.

[23] D. Ionita, M. Cristea, C. Gaina, Prediction of polyurethane behaviour via time-temperature superposition: meanings and limitations, Polym. Test. 83 (2020), https://doi.org/10.1016/j.polymertesting.2020.106340.

[24] J.D. Ferry, Viscoelastic Properties of Polymers, third ed., John Wiley&Sons, New York, 1980.

[25] D.J. Plazek, Bingham Medal Address: oh, thermorheological simplicity, wherefore art thou? J Rheol (N Y N Y) 40 (1996) (1995) 987–1014, https://doi.org/10.1122/1.550776.

[26] K. Schröter, S.A. Hutcheson, X. Shi, A. Mandanici, G.B. McKenna, Dynamic shear modulus of glycerol: corrections due to instrument compliance, J. Chem. Phys. 125 (2006) 214507, https://doi.org/10.1063/1.2400862.

[27] R. Mangal, S. Srivastava, L.A. Archer, Phase stability and dynamics of entangled polymer-nanoparticle composites, Nat. Commun. 6 (2015), https://doi.org/10.1038/ncomms8198.

[28] Y. Zhong, L. Yu, Q. Huang, Investigating the linear viscoelastic behaviour at high frequencies in the transition to glassy regime for polystyrene melts and solutions, Rheol. Acta (2022), https://doi.org/10.1007/s00397-022-01359-8.

[29] O.-V. Laukkanen, Small-diameter parallel plate rheometry: a simple technique for measuring rheological properties of glass-forming liquids in shear, Rheol. Acta 56 (2017) 661–671, https://doi.org/10.1007/s00397-017-1020-5.

[30] S. Katsourinis, E. Kontou, Comparing interconversion methods between linear viscoelastic material functions, Mech. Time-Dependent Mater. 22 (2018) 401–419, https://doi.org/10.1007/s11043-017-9363-y.

[31] F.R. Schwarzl, The numerical calculation of storage and loss compliance from creep data for linear viscoelastic materials, Rheol. Acta 8 (1969) 6–17, https://doi.org/10.1007/BF02321350.

[32] C. He, P. Wood-Adams, J.M. Dealy, Broad frequency range characterization of molten polymers, J Rheol (N Y N Y) 48 (2004) 711–724, https://doi.org/10.1122/1.1763943.

[33] W. You, W. Yu, Slow linear viscoelastic relaxation of polymer nanocomposites: contribution from confined diffusion of nanoparticles, Macromolecules 52 (2019) 9094–9104, https://doi.org/10.1021/acs.macromol.9b01538.

[34] B. Schroyen, D. Vlassopoulos, P. Van Puyvelde, J. Vermant, Bulk rheometry at high frequencies: a review of experimental approaches, Rheol. Acta 59 (2020) 1–22, https://doi.org/10.1007/s00397-019-01172-w.

[35] T. Athanasiou, G.K. Auernhammer, D. Vlassopoulos, G. Petekidis, A high-frequency piezoelectric rheometer with validation of the loss angle measuring loop: application to polymer melts and colloidal glasses, Rheol. Acta 58 (2019) 619–637, https://doi.org/10.1007/s00397-019-01163-x.

[36] L. Szántó, R. Vogt, J. Meier, D. Auhl, E. Van Ruymbeke, C. Friedrich, Entanglement relaxation time of polyethylene melts from high-frequency rheometry in the megahertz range, J Rheol (N Y N Y) 61 (2017) 1023–1033, https://doi.org/10.1122/1.4998174.

[37] M. van Gurp, J.H.M. Palmen, Time-temperature superposition for polymer blends, Rheology Bulletin 67 (1998) 5–8.

[38] H.C. Booij, J.H.M. Palmen, Linear viscoelastic properties of a miscible polymer blend system, in: P. Moldenaers, R. Keunings (Eds.), Theoretical and Applied Rheology, Elsevier, Amsterdam, 1992, pp. 321–323, https://doi.org/10.1016/B978-0-444-89007-8.50132-5.

[39] K. Molnar, H. Kim, D. Chen, C.A. Helfer, G. Kaszas, G.B. McKenna, J.A. Kornfield, C. Yuan, J.E. Puskas, PolyDODT: a macrocyclic elastomer with unusual properties, Polym. Chem. 13 (2022) 668–676, https://doi.org/10.1039/D1PY01426A.

[40] A. Oseli, A. Aulova, M. Gergesova, I. Emri, Effect of temperature on mechanical properties of polymers, in: H. Altenbach, A. Öchsner (Eds.), Encyclopedia of Continuum Mechanics, Springer Berlin Heidelberg, Berlin, Heidelberg, 2019, pp. 1–20, https://doi.org/10.1007/978-3-662-53605-6_269-2.

[41] S. Bouvier, H. Haddadi, P. Levée, C. Teodosiu, Simple shear tests: experimental techniques and characterization of the plastic anisotropy of rolled sheets at large strains, J. Mater. Process. Technol. 172 (2006) 96–103, https://doi.org/10.1016/j.jmatprotec.2005.09.003.

[42] L.D.C. Ramalho, J.M.M. Dionísio, I.J. Sánchez-Arce, R.D.S.G. Campilho, J. Belinha, Analysis of stress singularity in adhesive joints using meshless methods, Eng. Anal. Bound. Elem. 137 (2022) 29–40, https://doi.org/10.1016/j.enganabound.2022.01.012.

[43] E. Oberg, F.D. Jones, H.L. Horton, H.H. Ryffel, Machinery's Handbook, 31st Edition, Inc. Industrial Press, New York, 2020.

[44] C. van't Hof, K.M.B. Jansen, G. Wisse, L.J. Ernst, D.G. Yang, G.Q. Zhang, H.J. L. Bressers, Novel shear tools for viscoelastic characterization of packaging polymers, Microelectron. Reliab. 47 (2007) 240–247, https://doi.org/10.1016/j.microrel.2006.09.032.

[45] F. Ondreas, J. Jancar, Temperature, frequency, and small static stress dependence of the molecular mobility in deformed amorphous polymers near their glass transition, Macromolecules 48 (2015) 4702–4716, https://doi.org/10.1021/acs.macromol.5b00550.
[46] C. Liu, J. He, E. van Ruymbeke, R. Keunings, C. Bailly, Evaluation of different methods for the determination of the plateau modulus and the entanglement molecular weight, Polymer (Guildf) 47 (2006) 4461–4479, https://doi.org/10.1016/j.polymer.2006.04.054.
[47] J.M. Dealy, D.J. Read, R.G. Larson, Structure and Rheology of Molten Polymers from Structure to Flow Behavior and Back Again 2 nd Edition, n.d.
[48] S. Trinkle, C. Friedrich, Van Gurp-Palmen-plot: a way to characterize polydispersity of linear polymers, Rheol. Acta 40 (2001) 322–328, https://doi.org/10.1007/s003970000137.
[49] Y. Masubuchi, Y. Doi, T. Uneyama, Entanglement molecular weight, Nihon Reoroji Gakkaishi 48 (2020) 177–183, https://doi.org/10.1678/rheology.48.177.
[50] J. Dealy, D. Plazek, Time-temperature superposition-a users guide, Rheology Bulletin 78 (2009) 16–31. https://www.researchgate.net/publication/284663363.
[51] H. Liu, R. Luo, Development of master curve models complying with linear viscoelastic theory for complex moduli of asphalt mixtures with improved accuracy, Construct. Build. Mater. 152 (2017) 259–268, https://doi.org/10.1016/j.conbuildmat.2017.06.143.
[52] A. Szuchács, T. Ageyeva, R. Boros, J.G. Kovács, Bonding strength calculation in multicomponent plastic processing technologies, Mater. Manuf. Process. 37 (2022) 151–159, https://doi.org/10.1080/10426914.2021.1948052.
[53] B. Robertson, R.L. Thompson, T.C.B. McLeish, I. Robinson, Theoretical prediction and experimental measurement of isothermal extrudate swell of monodisperse and bidisperse polystyrenes, J Rheol (N Y N Y) 61 (2017) 931–945, https://doi.org/10.1122/1.4995603.
[54] K.L. Kearns, J. Scherzer, M. Chyasnavichyus, D. Monaenkova, J. Moore, R. L. Sammler, T. Fielitz, D.A. Nicholson, M. Andreev, G.C. Rutledge, Measuring flow-induced crystallization kinetics of polyethylene after processing, Macromolecules 54 (2021) 2101–2112, https://doi.org/10.1021/acs.macromol.0c02477.